Journal of Alloys and Compounds 492 (2010) 166–172

Contents lists available at ScienceDirect

Journal of Alloys and Compounds

journal homepage: www.elsevier.com/locate/jallcom

Inhomogeneous evolution of microstructure in AZ91 Mg-alloy during high temperature equal-channel angular pressing

Jenő Gubicza[a,*], Krisztián Máthis[b], Zoltán Hegedűs[a], Gábor Ribárik[a], Attila L. Tóth[c]

[a] Department of Materials Physics, Eötvös Loránd University, Pázmány Péter sétány 1/A., H-1117 Budapest, Hungary
[b] Department of Metal Physics, Charles University, Ke Karlovu 5, 121 16 Praha 2, Czech Republic
[c] Research Institute for Technical Physics and Materials Science, P.O.Box 49, H-1525 Budapest, Hungary

ARTICLE INFO

Article history:
Received 16 October 2009
Received in revised form
18 November 2009
Accepted 19 November 2009
Available online 26 November 2009

Keywords:
Mg-alloys
Severe plastic deformation
Equal-channel angular pressing
Dislocations
Precipitation

ABSTRACT

The evolution of the microstructure in AZ91 Mg-alloy processed by equal-channel angular pressing (ECAP) at 543 K was investigated. The initial material was a supersaturated solid solution, therefore the severe plastic deformation and the precipitation occurred simultaneously. The precipitate morphology and the defect structure in the matrix were studied after 2 and 8 ECAP passes. As a result of ECAP, continuous precipitates formed instead of discontinuous ones usually observed at 543 K. After 2 passes of ECAP, both the size of precipitates and the solute atom concentration in the matrix showed a high level of inhomogeneity but after 8 passes the microstructure became more homogeneous. The precipitates coarsened with increasing the number of ECAP passes.

1. Introduction

The AZ91 magnesium alloy (the main alloying elements are 9 wt.% Al and 1 wt.% Zn) is very attractive in many applications due to its good castability, high strength to weight ratio and excellent corrosion resistance [1]. This alloy is often used as a raw material for structural components in automobile and aircraft industries. The relatively high strength of AZ91 alloy can be attributed to the hexagonal crystal structure of the Mg matrix and the plate-like $Mg_{17}Al_{12}$ precipitates. These precipitates usually formed during the slow cooling after casting or annealing of the quenched samples at high temperatures [2,3]. Depending on the heat-treatment conditions, the precipitation in a supersaturated AZ91 alloy can occur continuously and/or discontinuously [2–5]. The discontinuous precipitates have a lamellar structure growing form the grain boundaries and they develop solely at low temperatures (up to about 450 K) [6]. Continuous precipitates form in the grain interiors and they have smaller aspect ratios compared to discontinuous precipitates [6]. Continuous precipitates usually develop during annealing of a supersaturated alloy at temperatures higher than about 600 K [6]. At intermediate temperatures, both types of precipitation occur simultaneously [6,7]. The precipitate morphology has a significant effect on mechanical properties as fracture is mostly initiated along them [8,9] and the fine dispersion of precipitates could improve ductility at high temperature [10].

It was found in previous papers [11–14], that severe plastic deformation (SPD) carried out at high temperatures on AZ91 alloy resulted in a change of both the grain structure and the morphology of precipitates. One of the most often used SPD method is equal channel angular pressing (ECAP) as it can be applied on bulk samples having dimensions of several centimeters in all directions [15]. It was found that the shape of precipitates in the samples processed by ECAP at 553 and 623 K was spherical while the annealing of supersaturated alloys at the same temperatures without plastic deformation resulted in elongated (plate-like) precipitates [12]. This change in the precipitate morphology can be explained by the strong distortion in the SPD-processed matrix lattice due to dislocations that can preclude the formation of long coherent boundary between the matrix and the precipitates. Consequently, spherical shape of precipitates is more favorable energetically than plate-like shape [12]. The spherical morphology of precipitates yielded a better ductility at high temperatures leading to an improvement of the poor workability of AZ91 alloys [10,11]. Moreover, the ECAP at high temperatures also resulted in a reduction of the grain size and an increase in the dislocation density thereby increasing the strength of the alloy [11,16]. The small grain size also contributes to the promotion of superplastic deformation at higher strain rates and/or lower temperatures than those conventionally used for large

* Corresponding author. Tel.: +36 1 372 2876; fax: +36 1 372 2811.
E-mail address: gubicza@metal.elte.hu (J. Gubicza).

0925-8388/$ – see front matter © 2009 Elsevier B.V. All rights reserved.
doi:10.1016/j.jallcom.2009.11.150

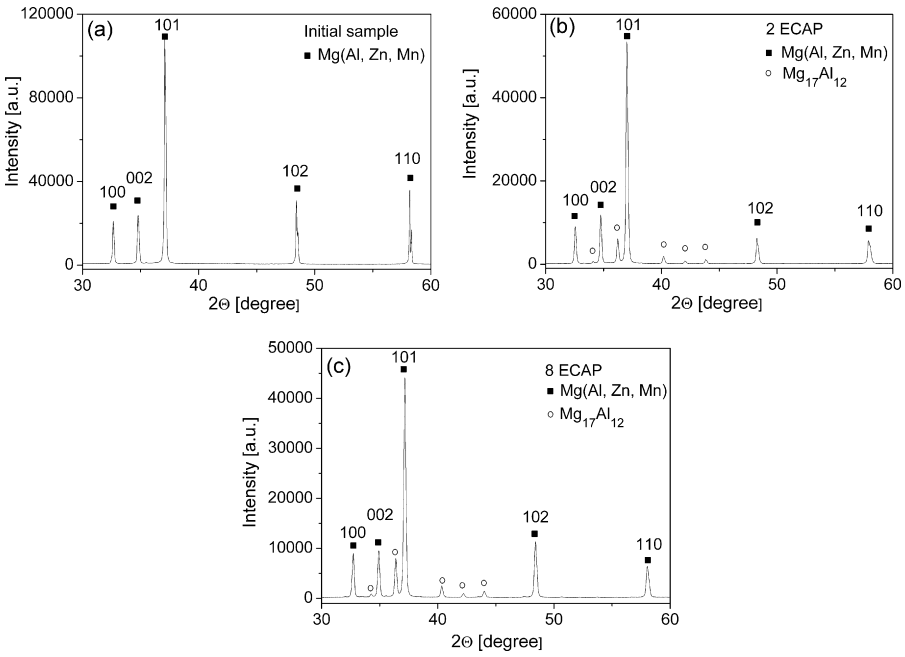

Fig. 1. Parts of the X-ray diffractograms showing the phase composition (a) in the initial state and after (b) 2 and (c) 8 passes.

grain size materials. The combination of high strength and good ductility in AZ91 alloys was also achieved by other SPD techniques, e.g. differential speed rolling [17,18]. A recent study [19] has shown that the grain refinement in AZ31 and ZK60 Mg-alloys processed by ECAP started at the initial grain boundaries therefore above a critical initial grain size (it is between 3 and 9 μm), inhomogeneous grain structure formed. In the present paper, we study the evolution of the microstructure in AZ91 magnesium alloy processed by ECAP at high temperature (543 K). Special attention is paid to the possible inhomogeneities in the matrix microstructure and the precipitation structure.

2. Experimental procedures

2.1. Sample preparation

The AZ91 alloy was produced by die-casting at Norsk Hydro, Oslo, Norway. The average chemical composition of the alloy was determined and guaranteed by the manufacturer as 89.81% Mg, 9.1% Al, 0.88% Zn, 0.18% Mn, 0.01% Si, 0.0045% Fe, 0.0011% Cu, 0.0007% Ni in wt.% and 2.08 ppm Be. The main alloying elements in at.% are 8.2% Al, 0.3% Zn and 0.1% Mn. The alloy was solution heat-treated for 18 h at 686 K. The heat-treated samples with dimensions of 10 mm × 10 mm × 60 mm were pressed through an ECAP die. The angle between the intersecting channels was 90° while the angle characterizing the outer arc of curvature of the channel intersection was 0°. The ECAP was carried out at a constant temperature of 543 K for 2 and 8 passes which correspond to the equivalent strains of 2.3 and 9.2, respectively [20]. The samples coated with molybdenum disulfide (MoS_2) were pressed at a rate of 5 mm/min using route C (i.e. the samples were rotated around their longitudinal axis by 180° after each pass) [21].

2.2. Experimental techniques for characterization of microstructure

The phase composition of the samples was studied by X-ray diffraction using a Philips Xpert θ–2θ powder diffractometer with Cu Kα radiation. The crystallite size and the dislocation structure in the matrix were investigated by X-ray peak profile analysis. The X-ray diffraction peak profiles were measured by a high-resolution diffractometer (Nonius FR591) with a rotating Cu anode and a Ge monochromator (Cu $K\alpha_1$ radiation, $\lambda = 0.15406$ nm). The instrumental broadening was much lower compared to the physical broadening of the profiles therefore instrumental correction was not applied.

The microstructure of the initial sample was studied by an Olympus optical microscope on the surface etched in a solution consists of 1 ml acetic picral, 4 ml acetic acid, 20 ml water and 75 ml methanol. The precipitate structure in the ECAP-processed specimens was investigated by scanning electron microscopy (SEM) using LEO XB 1540 and Tesla B525 microscopes. The studied surface of the samples was polished first by grinding papers and finally by water suspension containing 50 nm sized alumina particles. Some specimens were etched in a solution consists of 75 ml ethylene glycol, 1 ml HNO_3 and 24 ml H_2O for 15 s. Element maps were prepared by energy dispersive X-ray analysis (EDX) in the LEO XB 1540 microscope using a low value of accelerating voltage (5 kV) which ensures that the investigated volume has a relatively small diameter (about 300 nm).

2.3. Evaluation procedure of X-ray diffraction line profiles

The measured physical X-ray peak profiles of the matrix were evaluated by means of the convolutional multiple whole profile (CMWP) fitting procedure, described in detail in reference [22]. In this method, the experimental diffraction pattern is fitted by a theoretical diffraction pattern which is the sum of a background and the theoretical peak profiles for the matrix. For each reflection the theoretical line profile was obtained as the convolution of the theoretical size and strain profiles. The first 16 reflections of the Mg-matrix were evaluated. The peaks of the precipitates were included in the background of the pattern which was specified by a spline. The theoretical diffraction line profiles of the matrix were calculated on the basis of a model of the microstructure. In this model, the crystallites have spherical shape and log-normal size distribution and the lattice strains are assumed to be caused by dislocations. From the fitting of the experimental diffraction pattern by the theoretical one, the area-weighted mean crystallite size ($\langle x \rangle_{area}$ [23]) and the dislocation density (ρ) of the Mg-matrix were determined. It is noted that in Mg-alloys beside dislocations twins usually also contribute to plasticity. At the same time, when the effect of twins has been also included in the CMWP method [24], the twin probability obtained for the present ECAP-processed AZ91 alloys was under the sensitivity limit of X-ray line profile analysis. The twin probability is the relative frequency of twinned crystal planes along their normal vector and its detection limit by X-ray line profile analysis is about 0.1% that corresponds to a twin spacing of about 200 nm. This is in agreement with a recent X-ray study [25] which has shown that in AZ91 Mg-alloy processed by SPD, the value of twin probability was less than the sensitivity limit of X-ray line profile analysis. If there were twins in the microstructure of the present ECAP-processed AZ91 alloys, their average spacing is larger than the value corresponds to the detection limit of twins by X-rays (i.e. it is larger than 200 nm). Consequently, the assumption that the dislocations are the main sources of strain broadening of line profiles is realistic.

3. Results and discussion

Fig. 1 shows parts of the X-ray diffractograms illustrating the phase composition in the initial state and after 2 and 8 passes of ECAP. In the case of the initial sample (see Fig. 1a), only the peaks of the Mg-matrix are visible in the diffractogram. The positions of the diffraction lines are shifted to higher angles compared with pure Mg due to the reduction of the lattice parameters owing to the smaller size of solute atoms (e.g. Al) compared to Mg. The lack of peaks of

precipitates indicates that the majority of alloying elements are in solid solution. However, it is noted that Mn has a very low solubility in Mg and usually it forms Al_8Mn_5 intermetallic compound in the as-cast AZ91 structure and this phase is not soluble even during the solution heat-treatments. Probably, this compound exists in the initial sample after the solution heat-treatment, but its volume fraction was too low for the detection by X-ray diffraction analysis. The solute atom concentration was approximated from the lattice parameter. The lattice parameter a of the matrix having hexagonal crystal structure was determined by extrapolating the lattice parameters obtained from the $h\,k\,0$ reflections to $2\Theta = 180^\circ$ by the Nelson–Riley method [26]. As we could not separate the effect of the different alloying elements on the lattice parameter, therefore an effective total solute atom concentration (c_{sol}) was determined from the lattice parameter. Zn and Mn atoms have much smaller concentration than Al and they also reduce the lattice parameter as Al. Therefore c_{sol} was determined from the relationship between the lattice parameter of Mg(Al) solid solution and the Al concentration given in ref. [27]. The slightly larger size of Al compared to Zn and Mn most probably results in a systematically higher calculated solute atom concentration than the real value, but this deviation is about one order of magnitude smaller than the experimental error because of the very small amounts of Zn and Mn. For the initial sample $c_{sol} = 8.7 \pm 0.4$ at.% was obtained which agrees with the sum of the nominal alloying concentrations of Al, Zn and Mn in AZ91 alloy (8.6 at.%, see Section 2.1) within the experimental error. It is noted that the majority of Mn and a small fraction of Al are most probably in the Al_8Mn_5 intermetallic compound as it was mentioned above. The X-ray peak profiles for the initial specimen were as narrow as the instrumental broadening indicating that the crystallite size is larger and dislocation density is lower than the detection limits of the line profile analysis in our experiments (~800 nm and $\sim 10^{13}$ m^{-2} for the crystallite size and the dislocation density, respectively). Former transmission electron microscopy (TEM) [28] and optical microscopy [11] investigations showed that the mean grain size in the initial sample was 40 μm which is also verified by the optical micrograph presented in Fig. 2.

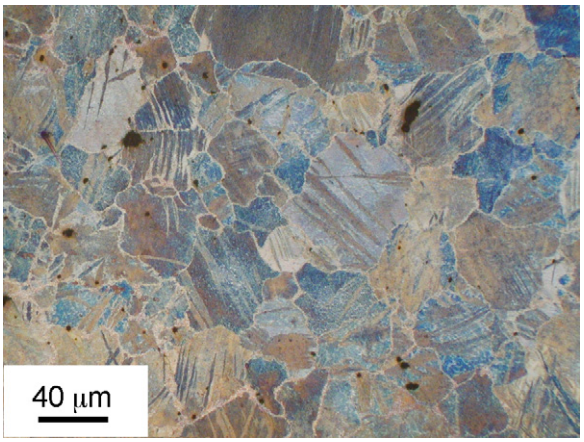

Fig. 2. Optical micrograph of the microstructure for the initial sample.

Fig. 1b and c shows that during 2 and 8 passes of ECAP carried out at high temperature, $Mg_{17}Al_{12}$ precipitates formed. The volume fraction of these precipitates was characterized by the ratio of the summed intensity under the $Mg_{17}Al_{12}$ peaks and for all the peaks in the diffractogram. It should be noted that this ratio does not give the $Mg_{17}Al_{12}$ phase content in the samples and it is only used to compare the two ECAP-processed specimens. The intensity ratios were 10.2% and 12.7% after 2 and 8 passes, respectively. It is noted that these values are close to the volume fraction (10%) of the $Mg_{17}Al_{12}$ phase at 543 K obtained from the equilibrium Mg–Al binary phase diagram [29]. As the intensity ratio determined after 2 passes is lower than after 8 passes only by about 20%, it can be concluded that the majority of precipitates has already formed after 2 passes of ECAP.

In the case of the samples processed by ECAP, the solute atom content of the matrix was determined from the X-ray diffraction peak positions, similarly as in the initial state. At the same time, careful investigations of the shape of peak profiles taken in the

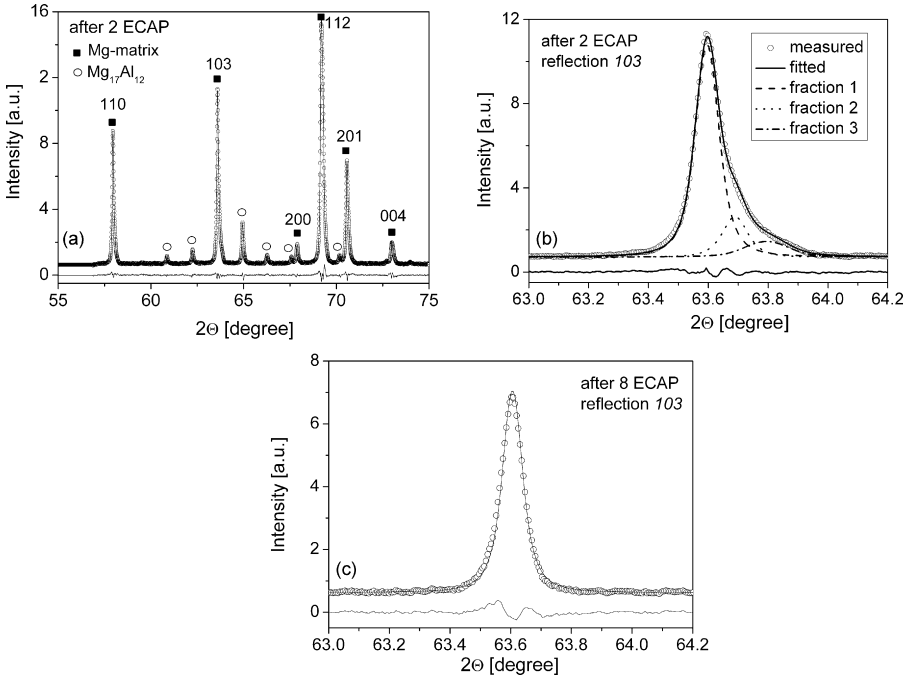

Fig. 3. (a) A part of the X-ray diffractogram fitted by the CMWP method for the sample processed by 2 ECAP passes. The magnified 1 0 3 reflection for (b) 2 and (c) 8 passes. The open circles and the solid line represent the measured and fitted patterns, respectively. In (b) the fitted peaks for the three fractions are also indicated by dashed and dotted curves. The difference between the measured and fitted patterns is at the bottom of the figures.

Table 1
The characteristic parameters of the Mg-matrix obtained by X-ray diffraction for the samples processed by 2 and 8 passes. c_{sol} is the solute atom concentration, $\langle x\rangle_{area}$ is the area-weighted mean crystallite size and is the dislocation density.

No. passes fraction	2 ECAP			8 ECAP
	1	2	3	1
c_{sol} [at.%]	4.8 ± 0.2	5.0 ± 0.2	5.3 ± 0.2	4.6 ± 0.2
$\langle x\rangle_{area}$ [nm]	193 ± 20	240 ± 30	81 ± 20	240 ± 30
ρ [10^{14} m^{-2}]	0.9 ± 0.2	1.4 ± 0.2	1.2 ± 0.2	1.6 ± 0.2

line profile experiments revealed that the solute atom concentration has a strong inhomogeneity in the specimen processed by 2 passes. Fig. 3a shows the fitting of a part of the diffractogram by the CMWP method after 2 passes. The open circles and the solid line represent the measured and the fitted patterns, respectively. In Fig. 3b, the 1 0 3 reflection is magnified from the pattern presented in Fig. 3a. This peak shows a strong asymmetry as the right tail of the profile decreases much slowly than the tail part at the left-hand side. The other peaks taken after 2 passes have similar shape. Peak asymmetry can be caused by different reasons, such as long range internal stresses, planar faults or chemical heterogeneities [30]. At the same time, in the former two cases the asymmetry is different for various reflections, i.e. the slowly decaying tail of the profile is on the smaller diffraction-angle part for some reflections and on the higher diffraction-angle part for other reflections depending on their $h\,k\,l$ indices [31,32,24]. For the alloy studied here, all the peaks show similar asymmetry independently of their $h\,k\,l$ indices (the slowly decaying tail is on the higher diffraction-angle part), which is characteristic for the asymmetry caused by chemical heterogeneities. Most probably, this type of asymmetry is caused by the high degree of inhomogeneity of solute atom concentration in the matrix which results in a variation in the lattice parameters of the Mg-matrix yielding to a splitting of the X-ray peaks.

Each asymmetric line profile can be evaluated by fitting it with the sum of several profile components having different Bragg-angles which correspond to the fractions of the matrix having slightly different lattice parameters. In order to evaluate these asymmetric line profiles, the CMWP method has been improved for fitting two or more sets of peaks of different crystalline phases. In the improved CMWP procedure, the experimental pattern can be fitted by the sum of theoretical patterns of various crystalline phases and a background spline. As the uncertainty of the fitting parameters increases with increasing the number of peak components fitted to a reflection, therefore a reasonable number of peak components should be selected for which the number of profile components is not very high and the fitting is well. In the case of the AZ91 alloy processed by 2 ECAP passes, the fitting of the line profiles was satisfactory only if each peak was assumed to consist of at least three profile components corresponding to three fractions in the matrix having different alloying compositions. Consequently, the diffraction pattern for the sample processed by 2 passes was fitted by a sum of three theoretical diffractograms corresponding to the three matrix fractions. The parameters of the microstructure as well as the peak positions and maxima of the three fractions were fitted by the CMWP method. Fig. 3b shows that the limitation of the number of fractions to three resulted in a satisfactory fitting to the experimental pattern. In Fig. 3b the fitted peaks for the three fractions are also indicated by dashed and dotted curves. It is noted that most probably the alloying concentration and therefore the lattice parameter change continuously, and the description of their distribution by three values is a strong simplification. Nevertheless, our procedure characterizes the inhomogeneity in the composition and the microstructure of the matrix. The alloying element concentration for the three fractions were determined by the same procedure as for the initial state and listed in Table 1. The solute atom concentration for the three fractions varies between 4.8 ± 0.2 and 5.3 ± 0.2 at.%. There are only slight differences between the concentrations of the various fractions, but as the peak positions are very sensitive to the alloying element content, therefore a splitting of the peaks were obtained. The variation of the solute atom concentration in the matrix is most probably a consequence of the inhomogeneous formation of precipitates. In the volumes, where the precipitation is far gone, the solute atom concentration in the matrix should be lower.

The relative amounts of the three fractions in the matrix were characterized by the relative intensities of their peak components summed up for all $h\,k\,l$ reflections. The relative amount of "fraction 1" having the smallest solute atom concentration is 73%. The other fractions with larger solute atom contents have much smaller amounts, namely 20% and 7% for "fraction 2" and "fraction 3", respectively. X-ray line profile analysis showed that in "fraction 1" having the smallest solute atom concentration, the dislocation density and the mean crystallite size are $(0.9 \pm 0.2) \times 10^{14}$ m^{-2} and 193 ± 20 nm, respectively. For the other two fractions containing more solute atoms, the dislocation density is slightly higher and moreover in the case of "fraction 3" the mean crystallite size is smaller than in "fraction 1" (see Table 1). This can be explained by the pinning effect of solute atoms on dislocations thereby hindering the dynamic recovery of the microstructure during high temperature ECAP-processing. It is noted that in severely deformed metals, the crystallite size measured by X-ray line profile analysis is usually smaller than the grain size obtained by TEM [30]. This phenomenon can be attributed to the fact that the crystallites are defined as the domains which scatter X-rays coherently. As the coherency of X-rays breaks even if they are scattered from volumes having quite small misorientations (1–2°), the crystallite size corresponds rather to the subgrain size in the severely deformed microstructures [33].

After 8 ECAP passes, the peak profiles show a high degree of symmetry (see Fig. 3c), indicating a strong reduction of the inhomogeneity in the solute atom concentration of the matrix. In this case, a single profile was enough for a satisfactory fitting of each peak. The solute atom concentration in the matrix is 4.6 ± 0.2 at.% that is the same as the value obtained from the equilibrium Mg–Al binary phase diagram at 543 K [29]. The mean crystallite size and the dislocation density are 240 ± 30 nm and $(1.6 \pm 0.2) \times 10^{14}$ m^{-2}, respectively. It should be noted that previous TEM experiments showed that the mean grain size decreased to 1.2 μm after 8 ECAP passes [34]. It was also revealed that in the latter sample the grains were divided into subgrains with the size of 100–200 nm which corresponds to the crystallite size determined by X-ray line profile analysis.

The crystallite size and dislocation density characteristic for the whole matrix in the sample processed by 2 passes can be calculated as the average of the values obtained for the three matrix fractions weighted by the relative amounts of these fractions. The average crystallite size and dislocation density are 195 ± 25 nm and $(1.0 \pm 0.2) \times 10^{14}$ m^{-2}, respectively. The crystallite size remained unchanged within the experimental error between 2 and 8 passes, while the dislocation density slightly increased. This indicates that the crystallite size saturated already after 2 passes while the dislocation density increased with further ECAP-processing at 543 K. The earlier saturation of the crystallite size compared to the dislocation density has been also observed for other metals, e.g. for Cu processed by ECAP at room temperature [35]. It is also noted that the dislocation density is relatively low despite the large value of strain applied during ECAP-processing. This can be attributed to the high homologous temperature of deformation (the ratio of absolute temperature of ECAP to absolute melting temperature was 0.59).

The SEM images in Fig. 4a and b shows etched surfaces of the specimen processed by 2 passes. The white objects in these figures correspond to the precipitates. Previous investigations [6]

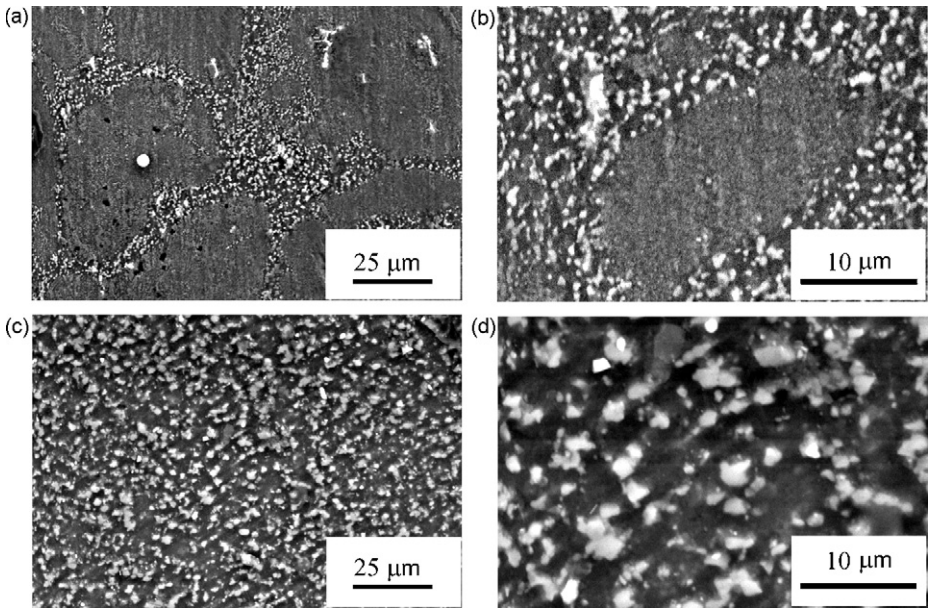

Fig. 4. SEM images taken on etched surfaces of the samples illustrating the precipitate microstructure after (a and b) 2 and (c and d) 8 passes.

have shown that the heat-treatment at 543 K without severe plastic deformation resulted in long plate-like discontinuous precipitates. The present results indicate that severe plastic deformation at high temperature yields the change of type of precipitates to rather spherical, continuous ones. This observation is in agreement with the results of a recent paper [12] where this effect was explained by the strong distortion in the SPD-processed matrix lattice that can preclude the formation of long coherent boundaries between the matrix and the precipitates and therefore spherical shape of precipitates is more favorable energetically than plate-like shape.

Fig. 4a and b shows that the precipitates have inhomogeneous distribution after 2 passes. Between the precipitated areas there are

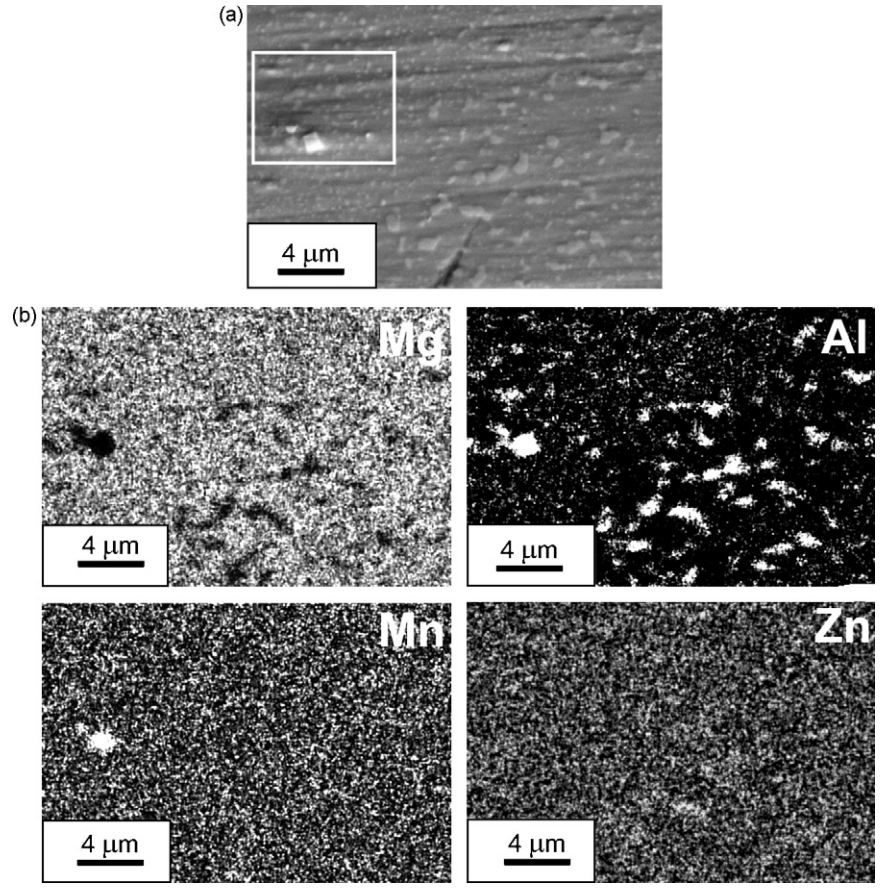

Fig. 5. (a) Secunder electron SEM image taken on a polished surface and (b) element maps for Mg, Al, Mn and Zn for the sample processed by 2 passes of ECAP. The white frame in (a) indicates the area shown in a higher magnification in Fig. 6.

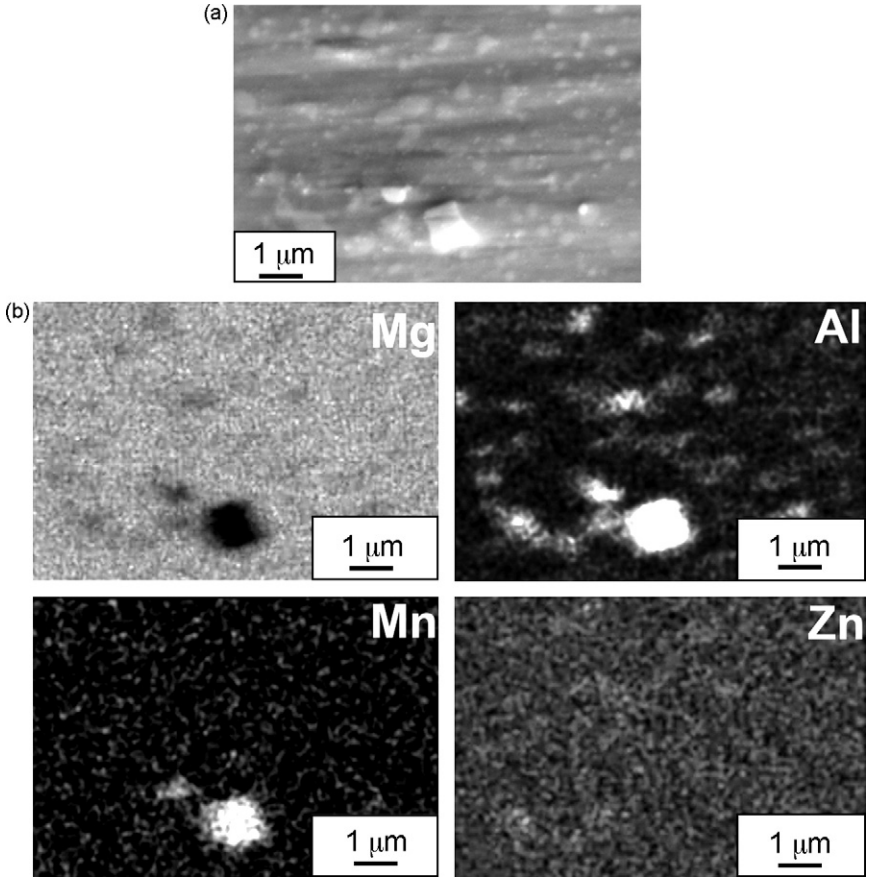

Fig. 6. The highly magnified area denoted by the white frame in Fig. 5. (a) SEM image and (b) element maps for Mg, Al, Mn and Zn.

regions where precipitates cannot be observed even in the image with higher magnification (see Fig. 4b). The majority of precipitates seem to be located at narrow zones which are most probably related to the boundaries of the initial grains. The areas observed to be precipitated and precipitate-free are comparable. At the same time, after 8 passes precipitation-free regions are not observed as can be seen in Fig. 4c and d. These SEM observations seem to be in contradiction to the results of X-ray diffraction where the intensity fraction of precipitates was smaller after 2 passes only by about 20% compared to the sample processed by 8 passes. This dichotomy can be solved considering the SEM images and the relating EDX element maps in Figs. 5 and 6 taken at high magnification on the polished surface of the sample processed by 2 passes. The areas having light grey contrast in the secondary electron image (SEI) of Fig. 5a correspond to the precipitates as it is confirmed by the Mg and Al element maps in Fig. 5b. The lighter the contrast in the map of a given element, the higher its concentration. The light grey areas in Fig. 5a are depleted from Mg and enriched in Al indicating that they correspond to the $Mg_{17}Al_{12}$ precipitates. On the right-hand side and at the bottom of the image in Fig. 5a, there is an area where large precipitates were formed. The mean size of the precipitates is about 0.5–1 μm which is the same as their size in the precipitated area in Fig. 4b. In the upper part of Fig. 5a, there are small precipitates. It is noted that there is a large (about 1 μm) grain in the left-hand side of Fig. 5a which is enriched with Mn. The composition of this grain is 56 at.% Al, 37 at.% Mn, 7 at.% Mg and 0.3 at.% Zn determined by EDX which is close to the stoichiometry of the phase Al_8Mn_5 observed previously in AZ91 alloy [36]. The area denoted by the white frame in Fig. 5a is enlarged in Fig. 6a and the corresponding element maps are presented in Fig. 6b. The areas having light grey contrast in Fig. 6a are the precipitates enriched in Al and depleted from Mg as it is proved by the corresponding element maps. The size of the smaller precipitates estimated from Fig. 6a is about 100–200 nm. The large precipitate enriched in Mn is also clearly visible in Fig. 6.

Figs. 5 and 6 prove that there is a high degree of inhomogeneity in the size of precipitates after 2 passes. There are volumes where the size of precipitates is large, about 0.5–1 μm, while in other regions only very small (100–200 nm) precipitates exist. Most probably, the latter regions appeared in Figs. 4a and b to be precipitate-free due to the lower magnification of these SEM images. This means that the majority of precipitates were formed already during the first 2 passes of ECAP, but in the grain interiors their size is much smaller than in the vicinity of the grain boundaries. The inhomogeneous development of precipitates is probably related to the different diffusion rate of solute atoms in Mg-matrix. The diffusion is faster at the grain boundaries than in the grain interiors, therefore the precipitates first form in the vicinity of the grain boundaries. As a consequence, after 2 passes the precipitates close to the boundary regions are larger than those developed in the interiors of the initial grains. Of course, during ECAP-processing a grain refinement occurs and the new grain boundaries also act as path for fast diffusion. A recent study [19] has shown that in Mg-alloys having an initial grain size larger than 10 μm, the grain refinement during ECAP started at the initial grain boundaries and the new small grains were arranged along the initial grain boundaries as a necklace. This observation also suggests that the precipitation is the fastest in the vicinity of the boundaries of the large initial grains and also in the interior of the smaller initial grains. At the same time, inside the large grains the precipitation is slower, although it is promoted by the relatively fast diffusion along dislocations formed during SPD. As a consequence, precipitates were

also formed inside the large initial grains but they have smaller size than those developed at the initial grain boundaries. It has been shown recently [19] that with increasing the number of ECAP passes, the grain refinement also occurred inside the large initial grains. This may contribute to the more homogeneous precipitate microstructure observed after 8 passes in our experiments (see Fig. 4c and d). Moreover, the size of the majority of precipitates is between 0.5 and 2.5 μm in the sample processed by 8 passes indicating a grain coarsening of precipitates with increasing the number of ECAP passes.

4. Conclusions

Supersaturated solid solution AZ91 alloy was processed by 2 and 8 passes of ECAP at high temperature (543 K). The severe plastic deformation and the precipitation occurred simultaneously during ECAP-processing. The evolution of the microstructure was studied by SEM and X-ray line profile analysis. The following conclusions have been drawn from the experimental results:

- It was found that SPD resulted in the formation of spherical continuous precipitates instead of long plate-like discontinuous ones which usually develop during heat-treatment at 543 K.
- After 2 passes there is a high degree of inhomogeneity both in the solute atom composition of the Mg-matrix and the size of $Mg_{17}Al_{12}$ precipitates. The majority of precipitates have been already formed during the first 2 passes of ECAP, but in the grain interiors their size was much smaller (100–200 nm) than in the vicinity of the grain boundaries (0.5–1 μm). At the same time, the matrix composition and the precipitate structure became more homogeneous after 8 passes.
- A coarsening of the precipitates was found with increasing the number of ECAP passes.

Acknowledgements

The authors are grateful for the support of the Hungarian TeT Foundation (KPI) under the contract No. CZ-4/2008. This work was supported by the Hungarian Scientific Research Fund, OTKA, Grant Nos. K67692 and K71594. This work is a part of the research program MSM 0021620834 that is financed by the Ministry of Education of the Czech Republic.

References

[1] B.L. Mordike, T. Ebert, Mater. Sci. Eng. A 302 (2001) 37–45.
[2] M.M. Avedesian, H. Baker (Eds.), ASM Specialty Handbook, Magnesium and Magnesium Alloys, The Materials Information Society, Materials Park, OH, 1999.
[3] C.H. Caceres, C.J. Davidson, J.R. Griffiths, C.L. Newton, Mater. Sci. Eng. A 325 (2002) 344–355.
[4] S. Maitrejean, M. Veron, Y. Brechet, G.R. Purdy, Scripta Mater. 41 (1999) 1235–1240.
[5] J.F. Nie, X.L. Xiao, C.P. Luo, B.C. Muddle, Micron 32 (2001) 857–863.
[6] K.N. Braszczynska-Malik, J. Alloys Compd. 477 (2009) 870–876.
[7] D. Duly, J.P. Simon, Y. Brechet, Acta Metall. Mater. 43 (1995) 101–106.
[8] G.L. Dunlop, W.P. Sequiera, M.S. Dargusch, G. Song, A. Atrens, T. Kittel, D.H. St John, A.K. Dahle, M. Murray, Proceedings of the 55th Meeting of the International Magnesium Association, 1998, p. 68.
[9] A.H. Feng, Z.Y. Ma, Scripta Mater. 56 (2007) 397–400.
[10] S. Kleiner, O. Beffort, A. Wahlen, P.J. Uggowitzer, J. Light Met. 2 (2002) 277–280.
[11] K. Máthis, J. Gubicza, N.H. Nam, J. Alloys Compd. 394 (2005) 194–199.
[12] K.N. Braszczynska-Malik, J. Alloys Compd. 487 (2009) 263–268.
[13] N.V. Ravi Kumar, J.J. Blandin, C. Desrayaud, F. Montheillet, M. Suéry, Mater. Sci. Eng. A 359 (2003) 150–157.
[14] A. Mussi, J.J. Blandin, L. Salvo, E.F. Rauch, Acta Mater. 54 (2006) 3801–3809.
[15] V.M. Segal, Mater. Sci. Eng. A 197 (1995) 157–164.
[16] B. Chen, D.-L. Lin, L. Jin, X.-Q. Zeng, C. Lu, Mater. Sci. Eng. A 483–484 (2008) 113–116.
[17] W.J. Kim, J.D. Park, W.Y. Kim, J. Alloys Compd. 460 (2008) 289–293.
[18] W.J. Kim, H.G. Jeong, H.T. Jeong, Scripta Mater. 61 (2009) 1040–1043.
[19] R.B. Figueiredo, T.G. Langdon, J. Mater. Sci. 44 (2009) 4758–4762.
[20] R.Z. Valiev, T.G. Langdon, Prog. Mater. Sci. 51 (2006) 881–981.
[21] K. Nakashima, Z. Horita, M. Nemoto, T.G. Langdon, Mater. Sci. Eng. A 281 (2000) 82–87.
[22] G. Ribárik, J. Gubicza, T. Ungár, Mater. Sci. Eng. A 387–389 (2004) 343–347.
[23] T. Ungár, J. Gubicza, G. Ribárik, A. Borbély, J. Appl. Cryst. 34 (2001) 298–310.
[24] L. Balogh, G. Tichy, T. Ungár, J. Appl. Cryst. 42 (2009) 580–591.
[25] L. Balogh, PhD thesis, Eotvos Lorand University, Budapest, 2009.
[26] J. Nelson, D. Riley, Proc. Phys. Soc. Lond. 57 (1945) 160–177.
[27] R.S. Busk, J. Met. 2 (1950) 1460–1464.
[28] A. Mussi, PhD Thesis, INP Grenoble, 2003.
[29] M. Hansen, K. Anderko, Constitution of Binary Alloys, McGraw-Hill, New York, 1958, p. 106.
[30] T. Ungár, J. Gubicza, Z. Kristallogr. 222 (2007) 114–128.
[31] H. Mughrabi, T. Ungár, W. Kienle, M. Wilkens, Phil. Mag. A 53 (1986) 793–813.
[32] L. Balogh, G. Ribárik, T. Ungár, J. Appl. Phys. 100 (2006) 023512.
[33] T. Ungár, G. Tichy, J. Gubicza, R.J. Hellmig, Powder Diffrac. 20 (2005) 366–375.
[34] K. Máthis, A. Mussi, Z. Trojanová, P. Lukáč, E.F. Rauch, J. Lendvai, Kovove Mater. (2003) 293–299.
[35] J. Gubicza, L. Balogh, R.J. Hellmig, Y. Estrin, T. Ungár, Mater. Sci. Eng. A 400–401 (2005) 334–338.
[36] D. Ohno, R. Mirkovic, R. Schmid-Fetzer, Acta Mater. 54 (2005) 3883–3891.